

Storage, form, and influencing factors of karst inorganic carbon in a carbonate area in China

Chaochao DU^{1,2}, Xiaoyong BAI^{1,3,5*}, Yangbing LI², Qiu TAN², Cuiwei ZHAO², Guangjie LUO⁴, Luhua WU¹, Fei CHEN^{1,5}, Chaojun LI¹, Chen RAN¹, Sirui ZHANG¹, Lian XIONG², Fengjiao SONG¹, Biqin XIAO², Zilin LI², Yingying XUE², Mingkang LONG¹, Qing LUO², Xiaoyun ZHANG², Minghui LI², Xiaoqian SHEN² & Shu YANG²

¹ State Key Laboratory of Environmental Geochemistry, Institute of Geochemistry, Chinese Academy of Sciences, Guiyang 550081, China;

² School of Geography and Environmental Sciences, Guizhou Normal University, Guiyang 550001, China;

³ CAS Center for Excellence in Quaternary Science and Global Change, Xi'an 710061, China;

⁴ Guizhou Provincial Key Laboratory of Geographic State Monitoring of Watershed, Guizhou Normal College, Guiyang 550018, China;

⁵ College of Resources and Environmental Engineering, Guizhou University, Guiyang 550025, China

Received February 14, 2023; revised September 28, 2023; accepted December 1, 2023; published online February 26, 2024

Abstract Carbonate rock chemical weathering carbon sinks reduce the rate of increase of the atmospheric CO₂ concentration and global warming. However, uncertainty still exists in the estimation results of carbonate rock chemical weathering carbon sink fluxes (CCSF), and the contributions of climate change and ecological restoration to the CCSF are not clear. To this end, we compiled published site data on ion concentrations in different watersheds in China and used a classical thermodynamic dissolution model to reassess the potential and spatial and temporal patterns of the CCSF in China from 1991 to 2020. We quantified the contributions of temperature (MAT), precipitation (MAP), evapotranspiration (ET), soil water (SM), and the normalized difference vegetation index (NDVI) to the CCSF. The results revealed that (1) China's CCSF was 22.76 t CO₂ km⁻² yr⁻¹, which was higher than the global average (15.77 t CO₂ km⁻² yr⁻¹). The total carbonate rock chemical weathering carbon sink (CCS) was 4772.67×10⁴ t CO₂, contributing 14.91% of the global CCS through a carbonate rock area of 252.98×10⁴ km². (2) China's CCSF decreased gradually from southeast to northwest, with values of 33.14, 12.93, and 7.27 t CO₂ km⁻² yr⁻¹ in the southern karst, Qinghai-Tibetan karst, and northern karst regions, respectively. (3) The overall CCSF in China exhibited an increasing trend from 1991 to 2020, with a rate of increase of 0.16 t CO₂ km⁻² yr⁻¹. (4) The contributions of the MAP, MAT, ET, SM, and NDVI to the CCSF were 63.3%, 3.02%, 27.5%, 3.1%, and 3.05%, respectively. Among them, the increase in precipitation was the main contributor to the increase in the CCSF in China over the last 30 years, while the enhancement of ET offset part of the positive contribution of the increase in precipitation to the CCSF. In conclusion, the results of this study provide a systematic quantification of the magnitude, the patterns, and the influencing factors of CCS over a long time series in China. The results are of great significance and provide a reference for the diagnosis and gap analysis of the national and global carbon neutrality capacities.

Keywords Carbonate rocks, Carbon sinks, Patterns, Influencing factors, Thermodynamic dissolution modeling

Citation: Du C, Bai X, Li Y, Tan Q, Zhao C, Luo G, Wu L, Chen F, Li C, Ran C, Zhang S, Xiong L, Song F, Xiao B, Li Z, Xue Y, Long M, Luo Q, Zhang X, Li M, Shen X, Yang S. 2024. Storage, form, and influencing factors of karst inorganic carbon in a carbonate area in China. *Science China Earth Sciences*, 67(3): 725–739, <https://doi.org/10.1007/s11430-023-1249-9>

* Corresponding author (email: baixiaoyong@vip.skleg.cn)

1. Introduction

Karst carbon sinks produced by the absorption of carbon dioxide in the air by carbonate rocks play an extremely important role in the carbon cycle (Liu et al., 2010, 2011; Pu et al., 2015; Cao et al., 2017; Liu et al., 2018; Zeng et al., 2019; Jia et al., 2022; Gao et al., 2022). The Fifth Assessment Report of the Intergovernmental Panel on Climate Change (IPCC) highlights that the carbon sink from the chemical weathering of carbonate rocks, as a technological pathway for removing atmospheric CO₂, ranks alongside terrestrial ecological processes, oceanic carbon sinks, and artificial capture and storage. Its magnitude may be as high as about 50% of the carbon sink of terrestrial vegetation (Jiang et al., 2011; Yuan, 2011). This point has been widely recognized in academic circles and has become the focus of social attention. In important documents such as China's Opinions on Doing a Good Job of Peak Carbon Reach and Carbon Neutrality published on 21 October 2021 and the Circular on the Action Plan for Peak Carbon Reach by 2030, published on 26 October 2021, karst carbon sinks have been emphasized many times, and it has been pointed out that karst carbon sinks are an important part of the country's efforts to realize the goal of the dual carbon strategy. The distribution area of carbonate rocks in China accounting for 15.64% of the global carbonate rock area (Song et al., 2017; An et al., 2018; Li et al., 2018, 2019; Li C J et al., 2019), carbon sinks has great potential. Therefore, clarifying the spatial pattern of carbonate weathering carbon sinks in the region, especially in China, and the contributions of its influencing factors will not only help to solve the problem of missing terrestrial carbon sinks but will also be of great significance and a reference for the diagnosis of carbon neutrality and gap analysis (Li H W et al., 2019; Bai et al., 2023).

How many carbon sinks have been chemically weathered from carbonate rocks in recent years? Where are these carbon sinks located? How do they change? How much climate change and ecological restoration affecting them has received widespread attention? Scholars from all over the world have explored the carbon sink potential of the chemical weathering of carbonate rocks at different spatial scales around this series of scientific questions using water-chemical runoff (Gaillardet et al., 1999; Xie et al., 2012). Computer simulation modeling (Suchet et al., 2003; Hartmann et al., 2009; Li et al., 2018), the global erosion model (GEM)-CO₂ (Qiu et al., 2004; Qin et al., 2013), the rock test piece method, and the diffusion boundary layer (DBL) model (Liu and Zhao, 2000) have been utilized to explore the carbon sink potential of the chemical weathering of carbonate rocks at different spatial scales, as well as the trend of its evolution. However, there are obvious differences in the magnitudes of carbon sinks calculated using different research methods, for example, the carbon sink potential of the

chemical weathering of carbonate rocks calculated based on the karst hydrochemistry method for carbonate rocks in the southern karst area, northern karst area, Qinghai-Tibetan karst area, and buried karst area of China is 1909.9×10^4 , 600.5×10^4 , 580.1×10^4 , and 608.6×10^4 t CO₂ yr⁻¹, respectively, and the total karst carbon sink is 3699.1×10^4 t CO₂ yr⁻¹ (Jiang et al., 2011). Based on the GEM-CO₂, it has been found that carbonate rocks in China consume about 4.72×10^7 t CO₂ per year due to weathering (Qiu et al., 2004), and the chemical weathering carbon sink of limestone calculated based on the thermodynamic dissolution model is 4171.52×10^4 t CO₂ (Li H W et al., 2019). On the global scale, the global carbon sink for carbonate rock weathering calculated using the water chemistry-runoff method is about 2.2 PgCO₂ yr⁻¹ (Liu et al., 2010, 2011). The global carbon sink for carbonate weathering calculated using a thermodynamic dissolution model is about 1.1 Pg CO₂ yr⁻¹ (Gombert, 2002). In addition, the dynamic karst system (carbonate-CO₂-H₂O system) is actively involved in the global carbon cycle through synergistic biological and inorganic karst processes and is highly sensitive to changes in climate and ecosystems (Jiang et al., 2011; Cao et al., 2017; ; Qin et al., 2021; Qiao et al., 2021; Xiao et al., 2022). Future carbonate weathering processes will be affected by a combination of climate and land use changes (Zeng and Liu, 2022; Behzad et al., 2023). Related studies have found that the main factor controlling the intensity of the carbonate chemical weathering carbon sinks in southwest China is runoff (Zeng, 2017), which contributes up to 70.36% (Sun et al., 2017; Li H W et al., 2019).

Many studies have been carried, laying a solid foundation for the study of the carbon sink effects and influencing factors of carbonate rock weathering processes. However, on the regional and national scales, most previous studies were based on positional observations or ion concentration data from the Global River Water Chemistry Database (GRWCD), which provides fewer monitoring stations with a regional distribution in China. This may lead to a large discrepancy in their results, and the contributions of the different driving factors are not yet clear. For this reason, we compiled the published ion concentration station data from different watersheds in China. Based on the thermodynamic dissolution model, we elucidated the magnitude of the chemical weathering carbon sinks of carbonate rocks in China from 1991 to 2020 and revealed their temporal and spatial variation patterns. The contributions of the changes in factors such as the precipitation (MAP), temperature (MAT), evapotranspiration (ET), normalized difference vegetation index (NDVI), and soil water (SM) to the carbonate rock chemical weathering carbon sink flux (CCSF) were evaluated in order to provide a reference for the diagnosis and gap analysis of the carbon neutral capacity in China and globally.

2. Materials and methods

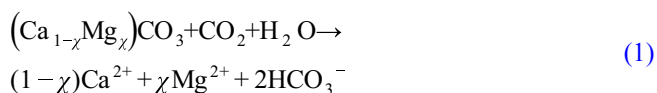
2.1 Data sources

The ET data for China were derived from the Harvard Davenport and the University of Montana Numerical Terra Dynamic Simulation Group (NTSG) (<https://www.ntsug.umt.edu/project/modis/>). The study period was 1991–2020, and the spatial resolution was 1 km×1 km. Monthly average temperature and precipitation data for China were obtained from the National Earth System Science Data Center. The spatial resolution was 1 km×1 km, and the time period was from January 1901 to December 2021 (Peng et al., 2019; Meng et al., 2021). These data have been widely used in studies on rock weathering carbon sinks and studies on ecological and environmental change (Myneni et al., 1997; Anyamba and Tucker, 2005; de Jong et al., 2013; Li H W et al., 2018; Zeng et al., 2019). Monthly data for NDVI were obtained from the National Earth System Science Data Center (<http://www.geodata.cn>), with a resolution of 1 km×1 km and a time period of 1982–2020. These data have been widely used to study time-series changes in regional vegetation (Myneni et al., 1997; Anyamba and Tucker, 2005; de Jong et al., 2013; Martin et al., 2017; Sedano et al., 2020). Monthly soil water data were derived from the Global Land Data Assimilation System (<https://ldas.gsfc.nasa.gov/gldas/>), with a time period of 1979–2020 and a spatial resolution of 1 km×1 km. The distribution and zoning of carbonate rocks in China were obtained from 1:2.5 million geological maps provided by the Geological Survey of China (Li and Luo, 1983; Ye et al., 2017). The Chinese regional rock data were extracted according to the attribute types, and we determined that the area of carbonate rocks in China was 252.98×10⁴ km², which is close to the areas reported in related studies (Li et al., 2018; Zeng and Liu, 2022). Riverine ion concentration data from 96 monitoring stations in the Chinese region were compiled through a literature review (Appendix 1.1, <https://link.springer.com>). Using data assimilation methods, all of the raw data were adjusted to the same spatial resolution (0.05°) (Table 1).

2.2 Research methods

2.2.1 Calculation of chemical weathering of carbonate rock carbon sinks

The maximum potential dissolution model is based on the assumption that carbonate areas reach dissolution equilibrium under local water, temperature, and CO₂ conditions (White, 1984). The equation is as follows:



Based on this equilibrium reaction, White (1984) proposed

a method for estimating the theoretical maximum annual dissolution rate of carbonate rocks, which is known as the maximal potential dissolution (MPD). The calculation formula is as follows:

$$D_{\max} = 10^6(\text{MAP} - \text{ET}) \cdot (K_s K_1 K_0 / 4K_2 \gamma_{\text{Ca}^{2+}} \gamma_{(\text{HCO}_3^-)^2})^{1/3} (p\text{CO}_2)^{1/3}, \quad (2)$$

where MAP and ET are the rainfall (mm yr⁻¹) and total ET, respectively. $\gamma_{\text{Ca}^{2+}}$ and $\gamma_{\text{HCO}_3^-}$ are the activity coefficients for Ca²⁺ and HCO₃⁻ ions in water, respectively (Appendix 1.2). K_s is the calcite solubility product constant, K_1 is the equilibrium constant for the hydration of CO₂ and its dissociation into HCO₃⁻, K_0 is the equilibrium constant for the dissolution of CO₂ in water, and K_2 is the equilibrium constant for formation (Plummer and Busenberg, 1982; Gombert, 2002) (Appendix 1.3). $p\text{CO}_2$ is the partial pressure of CO₂ in the soil or aquifer (Appendix 1.4).

2.2.2 Multiple linear regression

Multiple linear regression (MLR) is widely used to study the correlation between a dependent variable and multiple independent variables (Li, 2020). In this study, the ion concentration coefficients calculated according to the Debye-Hückel formula were subjected to MLR of the MAP, MAT, ET, NDVI, and SM at the corresponding monitoring stations. The results reveal that there are good correlations between $\gamma_{\text{Ca}^{2+}}$ and $\gamma_{\text{HCO}_3^-}$ and the MAP, MAT, ET, NDVI, and SM significance levels of $p < 0.01$. As a result, regression equations between $\gamma_{\text{Ca}^{2+}}$ and $\gamma_{\text{HCO}_3^-}$ and the MAP, MAT, ET, NDVI, and SM were established. The ionic activity coefficients were inverted spatially using the regression equations between $\gamma_{\text{Ca}^{2+}}$ and $\gamma_{\text{HCO}_3^-}$ and the MAP, MAT, ET, NDVI, and SM. The regression equations are as follows:

$$\begin{aligned} \gamma_i &= \gamma(\text{MAP}, \text{MAT}, \text{ET}, \text{SM}, \text{NDVI}) + \varepsilon_i \\ &= (b_0 + b_1\text{MAP} + b_2\text{MAT} + b_3\text{ET} + b_4\text{SM} + b_5\text{NDVI}) \\ &\quad + \varepsilon_i, \end{aligned} \quad (3)$$

where $\gamma_{\text{Ca}^{2+}}$ and $\gamma_{\text{HCO}_3^-}$ spatial fitting results are represented, respectively. ε_i represents the fitting residual values. b_1 , b_2 , b_3 , b_4 , and b_5 are the MAP, MAT, ET, SM, and NDVI fitting coefficients, respectively. b_0 is a constant. See Table S3 of Appendix for specific fitting parameters.

2.2.3 Trend analysis method

Based on the least squares method for estimating linear trend values, the trend of the CCSF during 1991–2020 was analyzed using the year as the independent variable and the CCSF as the dependent variable. The core formula is as follows (Yu et al., 2015; Gong et al., 2021; Li et al., 2022; Xiao et al., 2023):

Table 1 Related parameters and sources of basic data

Data	Spatial resolution	Source
MAP	1 km×1 km	National Earth System Science Data Center (http://www.geodata.cn)
MAT	1 km×1 km	National Earth System Science Data Center (http://www.geodata.cn)
ET	1 km×1 km	Harvard Dataverse (https://dataverse.harvard.edu/dataset.xhtml?persistentId=doi:10.7910/DVN/ZGOUED)
SM	1 km×1 km	Global Land Data Assimilation System (https://ldas.gsfc.nasa.gov/gldas/)
NDVI	1 km×1 km	National Earth System Science Data Center (http://www.geodata.cn)
Ca ²⁺ , Mg ²⁺ , Na ⁺ , K ⁺ , CO ₃ ²⁻ , HCO ₃ ⁻ , SO ₄ ²⁻ and Cl ⁻ concentration	–	Literature data collection
Carbonate outcrop	1:2500000	China Geological Survey (https://www.cgs.gov.cn)

$$K = \frac{\sum_{j=1}^n M_j t_j - \frac{1}{n} \left(\sum_{j=1}^n M_j \sum_{j=1}^n t_j \right)}{\sum_{j=1}^n t_j^2 - \frac{1}{n} \left(\sum_{j=1}^n t_j \right)^2}, \quad (4)$$

where K is the linear trend value, n is the study period, t_j represents the year and M_j is the independent variable corresponding to year j . M_j decreases or increases to a significant level if the correlation coefficient of the regression equation passes the significant confidence level of 0.05 and 0.01 ($p < 0.05$ and $p < 0.01$). The method can be computed down to the image element scale and can vi-

sualise regions of increase and decrease, but there may be some error between the computed and actual values on the regions.

2.2.4 Contribution rate evaluation

Quantifying the contribution of climate change and ecological restoration to CCSF using MAP, MAT, ET, NDVI and SM data, assuming other impact factors are constant (Ge et al., 2021). The relative contribution of climate change and ecological restoration to CCSF is expressed in the following equation:

$$\text{Contr. CCSF} = \frac{|\Delta\text{Clim. MAP}|}{|\Delta\text{Clim. MAP}| + |\Delta\text{Clim. MAT}| + |\Delta\text{Clim. ET}| + |\Delta\text{Clim. SM}| + |\Delta\text{Clim. NDVI}|} \times 100\%, \quad (5)$$

$$\text{Contr. CCSF} = \frac{|\Delta\text{Clim. MAT}|}{|\Delta\text{Clim. MAP}| + |\Delta\text{Clim. MAT}| + |\Delta\text{Clim. ET}| + |\Delta\text{Clim. SM}| + |\Delta\text{Clim. NDVI}|} \times 100\%, \quad (6)$$

$$\text{Contr. CCSF} = \frac{|\Delta\text{Clim. ET}|}{|\Delta\text{Clim. MAP}| + |\Delta\text{Clim. MAT}| + |\Delta\text{Clim. ET}| + |\Delta\text{Clim. SM}| + |\Delta\text{Clim. NDVI}|} \times 100\%, \quad (7)$$

$$\text{Contr. CCSF} = \frac{|\Delta\text{Clim. NDVI}|}{|\Delta\text{Clim. MAP}| + |\Delta\text{Clim. MAT}| + |\Delta\text{Clim. ET}| + |\Delta\text{Clim. SM}| + |\Delta\text{Clim. NDVI}|} \times 100\%, \quad (8)$$

$$\text{Contr. CCSF} = \frac{|\Delta\text{Clim. SM}|}{|\Delta\text{Clim. MAP}| + |\Delta\text{Clim. MAT}| + |\Delta\text{Clim. ET}| + |\Delta\text{Clim. SM}| + |\Delta\text{Clim. NDVI}|} \times 100\%, \quad (9)$$

In the formula, Cont.CCSF represents the contribution rate of climate factors to CCSF, and Clim.MAP, Clim.MAT, Clim.ET, Clim.SM, Clim.NDVI represents the partial correlation coefficients of precipitation, temperature, potential evapotranspiration, soil water, NDVI and other hydrological climate factors to CCSF.

3. Results

3.1 Spatial distribution of carbonate rock chemical weathering carbon sinks

China's CCSF was 22.76 t CO₂ km⁻² yr⁻¹ from 1991 to 2020, of which 33.14, 12.93, and 7.27 t CO₂ km⁻² yr⁻¹ were located

in the southern karst region, Qinghai-Tibetan karst region, and northern karst region, respectively. In the spatial distribution, the CCSF gradually decreased from southeast to northwest (Figure 1a). The areas with high CCSF values were mainly located in the southern karst areas with high water-heat fluxes. For example, Taiwan Province had the highest annual average CCSF and CCS values of $154.26 \text{ t CO}_2 \text{ km}^{-2} \text{ yr}^{-1}$ and $49.17 \times 10^4 \text{ t CO}_2$, respectively. In addition, the annual average CCSF was greater than $40 \text{ t CO}_2 \text{ km}^{-2} \text{ yr}^{-1}$ in Guangdong, Fujian, Jiangxi, Zhejiang, Anhui, Guangxi, and Hunan provinces. The low value areas were mainly distributed in the northern karst area. For example, the CCSF and CCS values in Ningxia were only $1.85 \text{ t CO}_2 \text{ km}^{-2} \text{ yr}^{-1}$ and $1.06 \times 10^4 \text{ t CO}_2$, respectively (Table 2). Latitudinally, the CCSF exhibited a fluctuating decreasing trend from low to high latitudes, and the high values were concentrated between 22°N and 25°N (Figure 1b). This region was also the most active region of the weathering processes of carbonate rocks in the southern karst area, with

a CCSF of $65 \text{ t CO}_2 \text{ km}^{-2} \text{ yr}^{-1}$.

Among the countries with major global carbonate distributions, China's CCSF is second only to that of Russia ($25.34 \text{ t CO}_2 \text{ km}^{-2} \text{ yr}^{-1}$), is higher than those of the United States ($17.53 \text{ t CO}_2 \text{ km}^{-2} \text{ yr}^{-1}$), Brazil ($16.76 \text{ t CO}_2 \text{ km}^{-2} \text{ yr}^{-1}$), Canada ($12.43 \text{ t CO}_2 \text{ km}^{-2} \text{ yr}^{-1}$), and India ($10.93 \text{ t CO}_2 \text{ km}^{-2} \text{ yr}^{-1}$). It is also higher than the CCSF of Slovenia ($7.59\text{--}16.50 \text{ t CO}_2 \text{ km}^{-2} \text{ yr}^{-1}$), the average global CCSF ($7.59\text{--}16.50 \text{ t CO}_2 \text{ km}^{-2} \text{ yr}^{-1}$), and other countries with CCSF (Figure 1c) (Gaillardet et al., 1999; Li et al., 2018; Zeng et al., 2019). China's CCS is $4772.67 \times 10^4 \text{ t CO}_2 \text{ yr}^{-1}$, which is relatively low compared to the CCSs in Canada ($19946.7 \times 10^4 \text{ t CO}_2$), the United States ($15924.3 \times 10^4 \text{ t CO}_2$), and France ($5742 \times 10^4 \text{ t CO}_2$) (Xiong et al., 2022). Although the area of carbonate rocks in China only accounts for 15.64% of the global carbonate rock area, it provides 14.91% of the karst carbon sinks in the global CCS ($3.2 \times 10^8 \text{ t CO}_2$) (Zeng et al., 2019), and thus, it makes an important contribution to the achievement of China's and even global

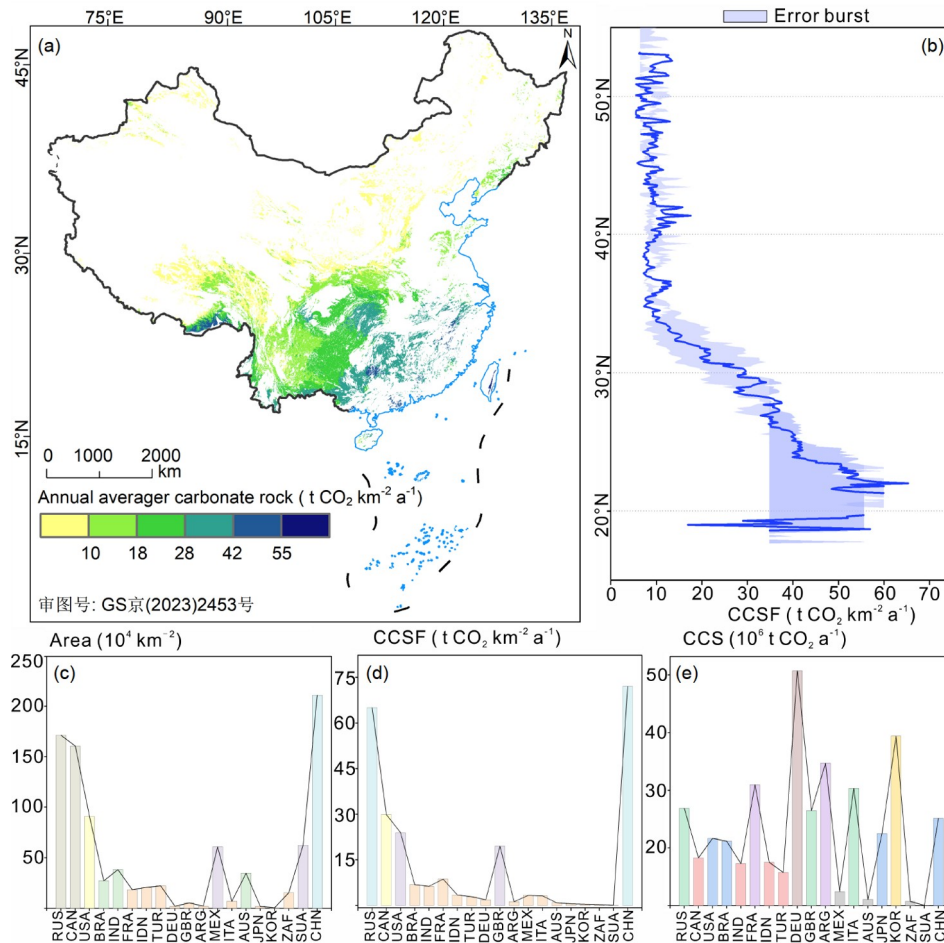


Figure 1 (a) Spatial distribution of carbonate rocks chemical weathering carbon sinks. (b) Latitudinal distribution of annual average carbonate chemical weathering carbon sinks. (c) Comparison of carbonate area distribution in different study areas. (d) Comparison of weathered carbon convergence amount of carbonate rock. (e) Comparison diagram of the total carbonate rock amount. CHN, China; JPN, Japan; KOR, South Korea; IND, India; GBR, United Kingdom; FRA, France; DEU, Germany; RUS, Russia; USA, United States; CAN, Canada; MEX, Mexico; ZAF, South Africa; SUA, Saudi Arabia; TUR, Türkiye; ITA, Italy; IDN, Indonesia; BRA, Brazil; AUS, Commonwealth of Australia; ARG, Republic of Argentina.

Table 2 Statistical table of carbonate rocks carbon sinks by province in China

Regions	CCSF (t CO ₂ km ⁻² yr ⁻¹)	Area (10 ⁴ km ²)	CCS (10 ⁴ t CO ₂ yr ⁻¹)	Proportion (%)
Yunnan	23.19	21.46	497.68	12.65
Sichuan	19.91	19.23	382.87	9.80
Xizang	16.68	63.00	1050.78	9.68
Hunan	43.28	8.39	362.94	9.39
Guangxi	43.95	11.54	507.30	13.27
Guizhou	30.63	14.73	451.21	11.51
Xinjiang	4.13	28.44	117.51	0.51
Hubei	31.45	8.41	264.44	6.88
Jiangxi	51.82	3.21	166.38	4.26
Zhejiang	49.40	1.12	55.44	1.39
Chongqing	34.82	6.03	209.85	5.30
Guangdong	56.01	2.22	124.26	3.03
Shaanxi	13.15	6.98	91.82	2.41
Shanxi	5.50	4.60	25.26	0.54
Anhui	40.27	1.22	49.26	1.24
Qinghai	5.19	15.87	82.35	0.93
Gansu	4.99	7.69	38.37	0.47
Fujian	50.70	0.82	41.43	1.05
Shandong	15.28	1.89	28.86	0.73
NeiMonggol	3.19	13.05	41.58	0.52
Henan	12.50	2.68	33.47	0.89
Jilin	13.98	1.15	16.11	0.42
Heibe	4.78	2.85	13.60	0.23
Jiangsu	19.35	0.33	6.40	0.15
Heilongjiang	7.91	1.41	11.11	0.29
Beijing	3.28	0.46	1.51	0.02
Liaoning	14.47	2.76	39.87	0.90
Ningxia	1.85	0.57	1.06	0.01
Tianjin	3.50	0.05	0.17	0.00
Shanghai	0.00	0.00	0.00	0.00
Hainan	35.20	0.30	10.60	0.26
Taiwan	154.27	0.32	49.17	1.26
Hong Kong	0.00	0.00	0.00	0.00
Macao	0.00	0.00	0.00	0.00
Total	22.76	252.98	4772.67	100.00

carbon neutrality goals.

3.2 Spatial and temporal evolution of carbonate rock chemical weathering carbon sinks

The CCSF in China exhibited an increasing trend during the study period. The areas that experienced an increase ac-

counted for about 79.91% of the overall area, and the rate of increase was 0.16 t CO₂ km⁻² yr⁻¹. The results correspond with the relevant studies (Raymond et al., 2008; Gislason et al., 2009; Drake et al., 2018). The areas with significant increases in the spatial distribution were mainly located in the southern karst areas with better hydrothermal conditions, such as Hainan, Sichuan, Guizhou, Yunnan, and other areas

with active chemical weathering of carbonate rocks. The CCSF growth rates in these areas were 0.81, 0.34, 0.32 t CO₂ km⁻² yr⁻¹, and 0.28 t CO₂ yr⁻¹, respectively (Figure 2a). In 24.09% of the areas, the CCSF exhibited a decreasing trend. These areas were mainly distributed in the southwestern part of Hunan, the northwestern part of Hubei, most of Jiangxi Province, and the southeastern part of Xizang autonomous region. These decreases were mainly due to the significant decrease in rainfall and the increase in evaporation, which decreased the water volume and dissolved CO₂ in the carbonate rock area and eventually led to the decreasing trend of the CCSF. The areas with significant vertical increase were mainly distributed in the low latitude region, and the values decreased from the low latitudes to high latitudes. The increase in the CCSF was most pronounced near 15°N–20°N, with a rate of 0.8 t CO₂ km⁻² yr⁻¹,

followed by 25°N–28°N, with a CCSF growth rate of about 0.4 t CO₂ km⁻² yr⁻¹. In the southern karst region, between 30°N and 45°N, the CCSF exhibited a decreasing trend (Figure 2b). Temporally, the CCSF was relatively high in 1994, 2002, 2008, 2015, 2016, and 2017, with values greater than 27 t CO₂ km⁻² yr⁻¹. The highest value (30 t CO₂ km⁻² yr⁻¹) occurred around 2015. In contrast, the CCSF was relatively low in 1995, 2009, 2011, and 2019, with values less than 20 t CO₂ km⁻² yr⁻¹. The lowest CCSF of 17.62 t CO₂ km⁻² yr⁻¹ occurred in 2011 (Figure 2c).

3.3 Correlation analysis between driving factors and carbonate rock chemical weathering carbon sinks

The correlations between the MAP, MAT, ET, NDVI, and SM and the CCSF in the carbonate rock areas in China were

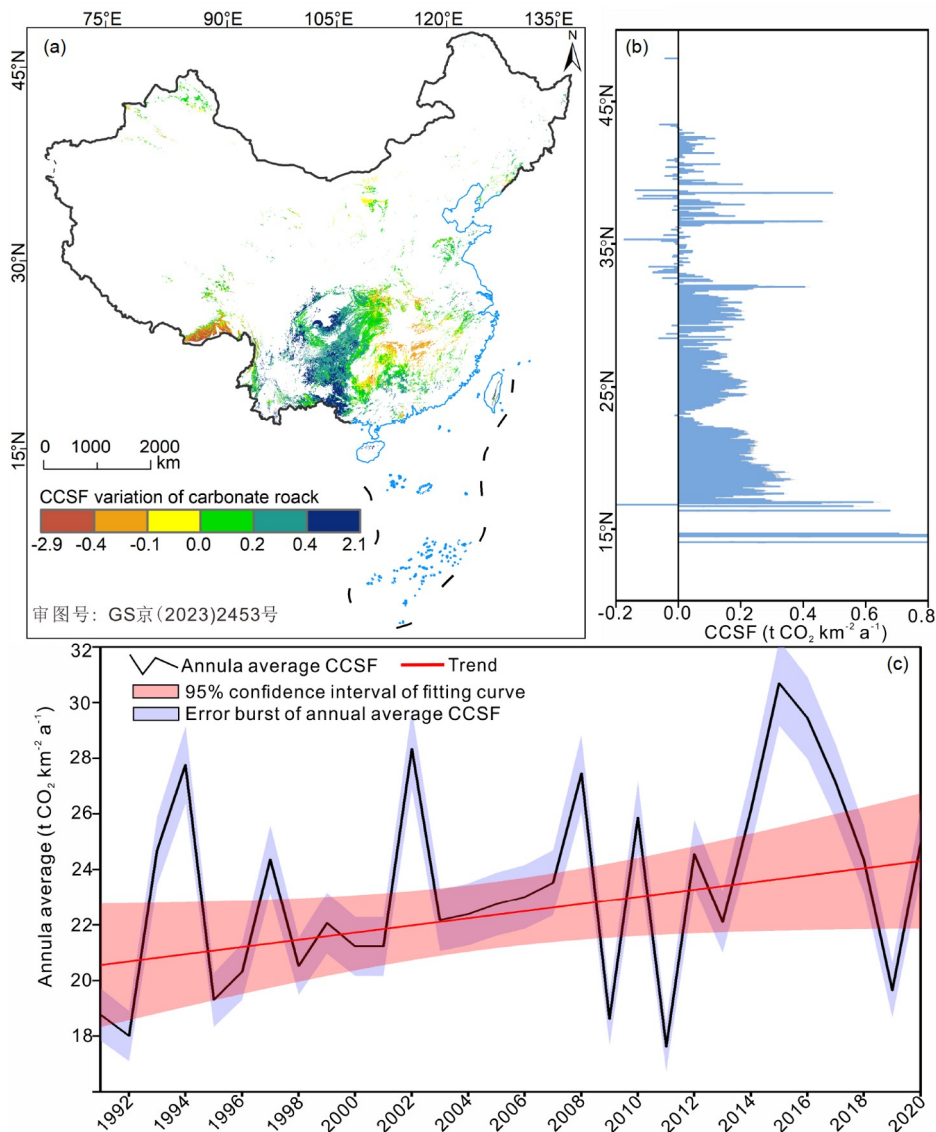


Figure 2 Characteristics of the spatial and temporal evolution of the chemical weathering carbon sinks in carbonate rocks. (a) Spatial evolutionary trends; (b) latitudinal evolutionary features; (c) annual average evolutionary trends.

explored via partial correlation analysis, and the mean values of their partial correlation coefficients were -0.001 , 0.58 , -0.42 , 0.014 , and -0.013 , respectively. The partial correlation coefficient between the MAT and CCSF revealed that 51.63% of the carbonate distribution areas exhibited a negative correlation between the MAT and the CCSF (Figure 3a), and these areas were mainly distributed in the southwestern karst region, indicating that the increase in MAT attenuated the CCSF in this region. The partial correlation coefficient between the MAP and CCSF revealed that the MAP was positively correlated with the CCSF in 95.40% of the districts and was negatively correlated with the CCSF in only 4.60% of the districts, indicating that the MAP had a significant promotive effect on the increase in the CCSF (Figure 3b). The partial correlation coefficient between the ET and CCSF revealed that there was a negative correlation between the ET and CCSF in 88.97% of the areas, indicating that the increase in ET had a strong inhibitory effect on the increase in CCSF, which mainly exhibited a negative correlation (Figure 3c). The SM was negatively correlated with the CCSF in 51.57% of the areas, mainly in the southern karst region. However, the SM was positively correlated with the CCSF in 48.43% of the areas, such as the Tibetan Plateau, where strong evaporation leads to a shortage of surface runoff and abundant SM provides sufficient water conditions for chemical weathering of carbonate rocks (Figure 3d). The NDVI responds to the vegetation growth status and vegetation cover (Martin et al., 2017; Sedano et al., 2020). The bias correlation analysis between the NDVI and CCSF revealed that the NDVI and CCSF were positively correlated in 53.43% of the area, mainly in the southern karst area, indicating that the improvement of the ecological environment promoted the chemical weathering of carbonate rocks in the southern karst area (Figure 3e). In conclusion, the rates of chemical weathering of the carbonate rocks in the different regions were controlled by a combination of factors. Therefore, it is not possible to analyze the influence of the changes in the magnitude of the CCSF using only a single factor, and the joint influence of multiple factors must be considered.

3.4 Evaluation of the contributions of driving factors to the carbonate rock chemical weathering carbon sink

To evaluate the relative importance of the MAP, SM, ET, and NDVI to the CCSF, the relative contributions of the MAP, MAT, ET, NDVI, and SM to the CCSF were quantified (Figure 4). The relative contributions of the MAP, MAT, ET, SM, and NDVI to the CCSF were 63.3%, 3.02%, 27.5%, 3.1%, and 3.05%, respectively. The area where the bias correlation coefficient between the MAP and CCSF was greater than 0 accounted for 95.40% (Figure 3f), indicating that the MAP was positively correlated with the CCSF; that

is, the increase in precipitation provided sufficient water for the chemical weathering of carbonate rocks, which was conducive to accelerating the chemical weathering process of the carbonate rocks. With a contribution rate of 63.3%, precipitation was the largest contributor to the CCSF among all of the factors considered. In contrast, the bias correlation coefficient between the ET and the CCSF was less than 0 in 88.97% of the areas, indicating that the ET and CCSF were mainly negatively correlated with each other, with a contribution rate of 27.5%, that is, with increasing evaporation, the chemical weathering process of the carbonate rocks was hindered to a certain extent, thus reducing the weathering rate of the carbonate rocks. The contributions of the SM, MAT, and NDVI to the CCSF were relatively small, and the areas with bias correlation coefficients greater than 0 and less than 0 were almost equal. This indicates that the contributions of the SM, MAT, and NDVI to the CCSF were different in regions with different geological backgrounds and climate types.

4. Discussion

4.1 Comparison of weathering carbon sink fluxes of different carbonate rocks

Carbonate rocks are mainly composed of limestone, dolomite, and mixed rocks, and based on a 1:2.5 million geological map, the area of carbonate rocks in China is $252.98 \times 10^4 \text{ km}^2$, of which the areas of limestone, dolomite, and mixed rocks are 184.50×10^4 , 7.08×10^4 , and $61.41 \times 10^4 \text{ km}^2$, accounting for 72.93%, 2.79%, and 24.27% of the carbonate distribution area in China, respectively. In terms of spatial distribution, they are mainly concentrated in the southwestern part of China and the Tibetan Plateau. The mineral composition of limestone is mainly CaCO_3 , while that of dolomite is mainly $\text{CaMg}(\text{CO}_3)_2$, which leads to a difference in the weathering carbon sink capacity due to the different compositions. The thermodynamic dissolution model establishes a relationship between the carbon sink fluxes of the chemical weathering of dolomite and limestone based on the relationship between the concentrations of HCO_3^- when the reactions reach equilibrium in their respective pure aqueous solution environments (Zeng et al., 2016, 2022). The CCSF in China was estimated to be $22.76 \text{ t CO}_2 \text{ km}^{-2} \text{ yr}^{-1}$, of which the CCSF of limestone, dolomite, and mixed rocks were 21.51, 23.57, and $25.59 \text{ t CO}_2 \text{ km}^{-2} \text{ yr}^{-1}$, respectively (Figure 5).

4.2 Comparison of carbon sink fluxes from carbonate rock weathering in different climate zones

According to the Köppen climate classification standard (Figure 6a), the Chinese region can be divided into 21 cli-

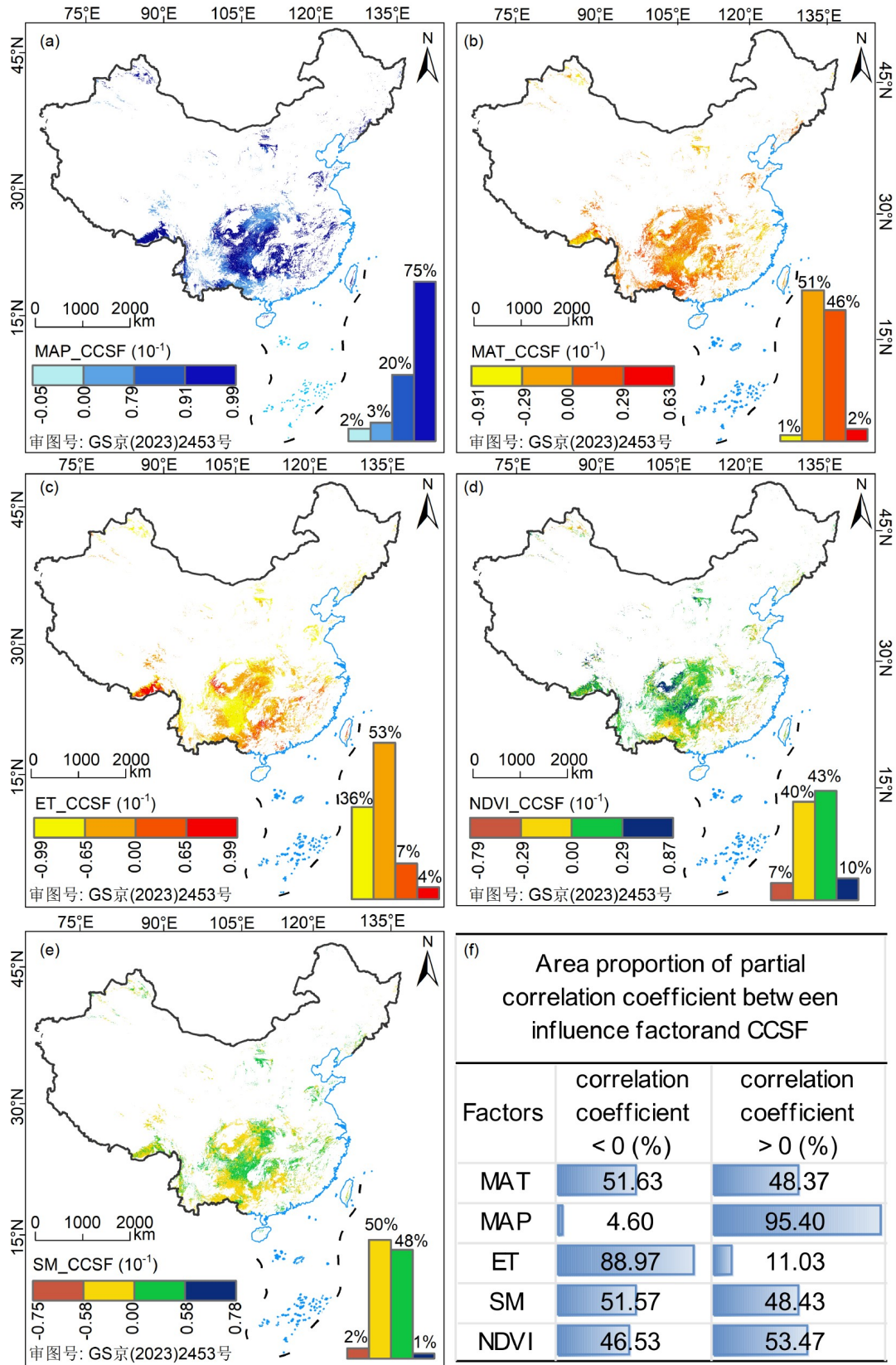


Figure 3 Driving factor correlation tests with carbonate chemical weathering carbon sinks. (a) Temperature and carbonate chemical weathering carbon sink correlation test; (b) precipitation and carbonate chemical weathering carbon sink correlation test; (c) potential evapotranspiration and carbonate chemical weathering carbon sink correlation test; (d) soil water and carbonate chemical weathering carbon sink correlation test; (e) test on correlation between NDVI and carbon sinks of carbonate chemical weathering.

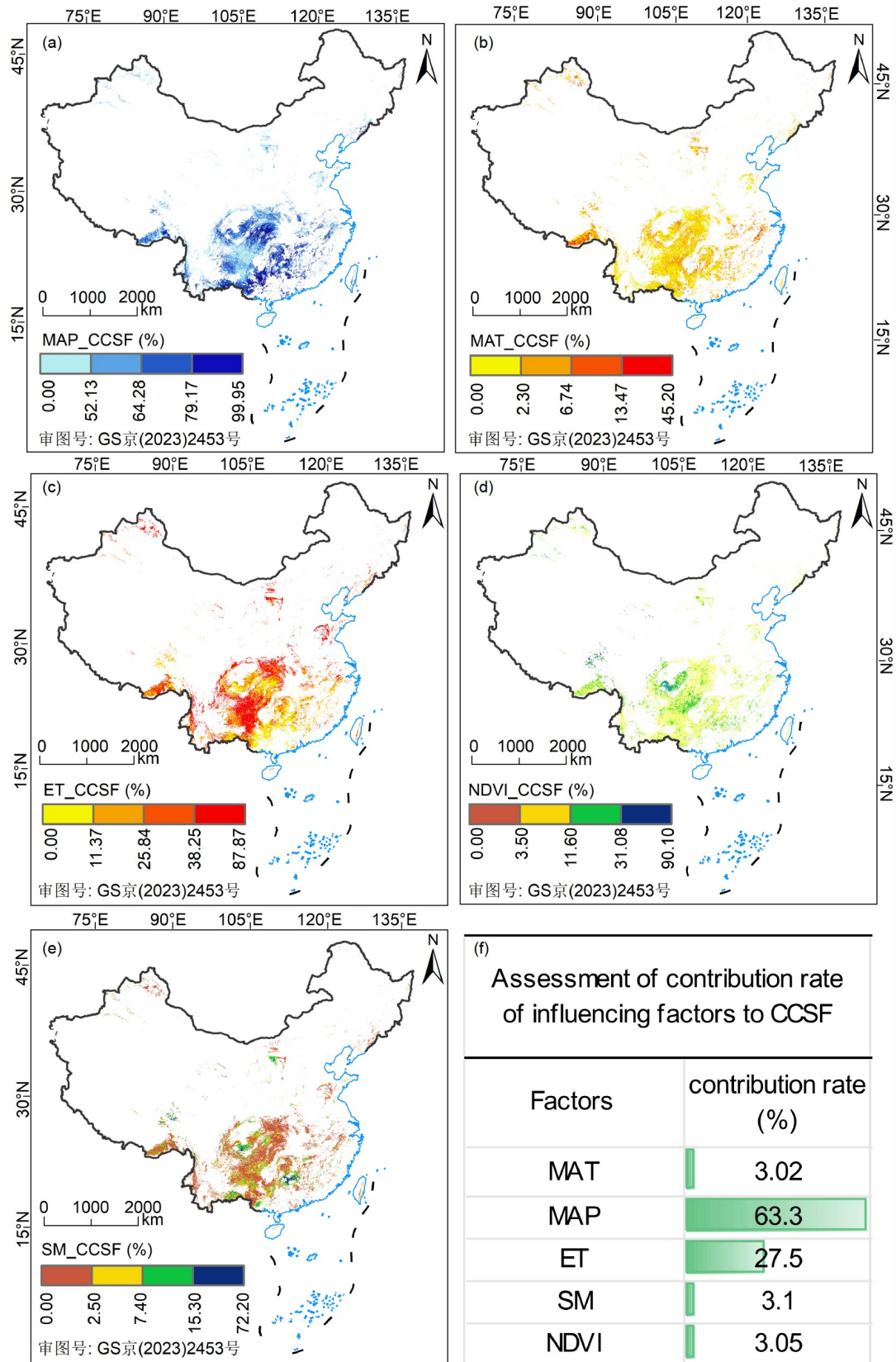


Figure 4 Contributions of driving factors to carbonate chemical weathering carbon sinks. (a) The contribution of temperature to the carbon sink of carbonate chemical weathering; (b) the contribution of precipitation to carbon sink of carbonate chemical weathering; (c) the contribution of potential evapotranspiration to carbon sink of carbonate chemical weathering; (d) the contribution of 0–10 cm soil water to carbon sink of carbonate chemical weathering; (e) the contribution of NDVI to carbon sink of carbonate chemical weathering.

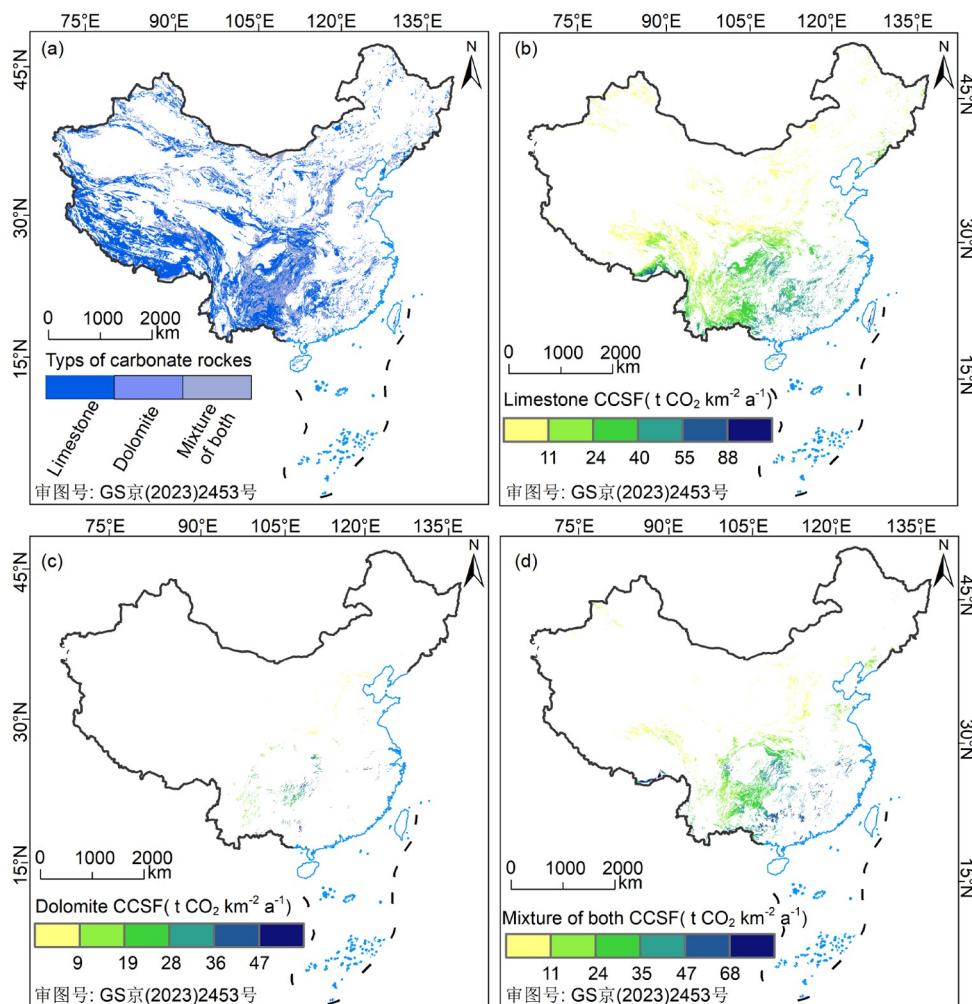


Figure 5 Spatial and temporal distribution of carbonate rocks types and chemical weathering carbon sinks in different carbonate rocks. (a) carbonate rocks types; (b) limestone chemical weathering carbon sinks; (c) dolomite chemical weathering carbon sinks; (d) mixed rocks chemical weathering carbon sinks.

matic zones, including the southern subtropical monsoon rainforest climate, tropical rainforest and monsoon rainforest climate, meso-subtropical monsoon broadleaf evergreen forest climate, northern subtropical monsoon deciduous broadleaf and broadleaf evergreen forest climate, and temperate broadleaf deciduous forest climate. By comparing the magnitudes of the CCSF in the different climate zones (Figure 6b), we found that the CCSF in the southern subtropical monsoon rainforest climate zone was $42.99 \text{ t CO}_2 \text{ km}^{-2} \text{ yr}^{-1}$, that in the tropical rainforest and monsoon rainforest climate zone was $42.04 \text{ t CO}_2 \text{ km}^{-2} \text{ yr}^{-1}$, and that in the mid-subtropical monsoon broadleaf evergreen forest climate zone was $33.94 \text{ t CO}_2 \text{ km}^{-2} \text{ yr}^{-1}$, which were all higher than the national average CCSF ($22.76 \text{ t CO}_2 \text{ km}^{-2} \text{ yr}^{-1}$). These were the regions with the highest CCSF among the 21 climate zones in China. In contrast, the climatic zones with the lowest CCSF were the cold steppe climate zone ($1.17 \text{ t CO}_2 \text{ km}^{-2} \text{ yr}^{-1}$), the mid-temperate continental desert-steppe climate zone

($1.91 \text{ t CO}_2 \text{ km}^{-2} \text{ yr}^{-1}$), and the temperate desert climate zone ($3.31 \text{ t CO}_2 \text{ km}^{-2} \text{ yr}^{-1}$). Overall, the tropics served as a concentrated distribution area for the CCSF, which gradually decreased from south to north. Relevant studies have found that globally, the CCSF also exhibits an increase from north to south among the climate zones, with an overall decreasing trend from the low-latitude tropical regions to the high-latitude regions. For example, it was found that the global CCSF was the highest in the tropics (about $101.42 \text{ t CO}_2 \text{ km}^{-2} \text{ yr}^{-1}$) and lower in the cold and polar regions at high latitudes ($26.8 \text{ t CO}_2 \text{ km}^{-2} \text{ yr}^{-1}$) (Goldscheider et al., 2020). The tropical rainforest climate zone has a CCSF of $773.67 \text{ t CO}_2 \text{ km}^{-2} \text{ yr}^{-1}$, which is about 2.5 times higher than that of the temperate oceanic climate zone ($311.67 \text{ t CO}_2 \text{ km}^{-2} \text{ yr}^{-1}$). The humid subtropical climate zone has the lowest carbon sink flux (only $40.33 \text{ t CO}_2 \text{ km}^{-2} \text{ yr}^{-1}$) (Li et al., 2018). In the major global basins, the CCSF is $49.87 \text{ t CO}_2 \text{ km}^{-2} \text{ yr}^{-1}$ in the tropics, followed by $45.1 \text{ t CO}_2 \text{ km}^{-2} \text{ yr}^{-1}$ in the warm temperate

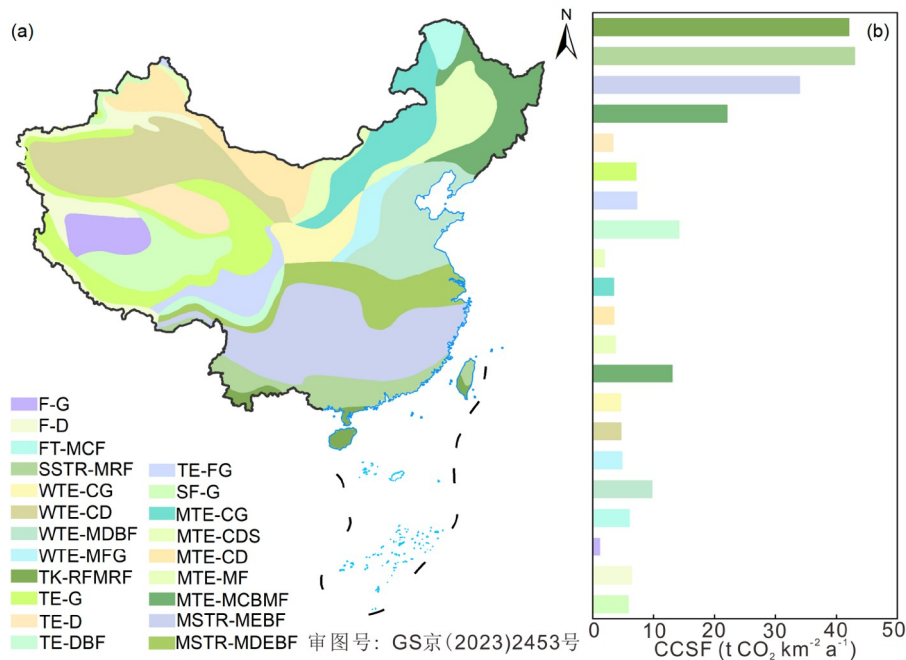


Figure 6 Distribution of climatic zones in China and carbon sink levels by climatic zone. (a) Distribution of climatic zones and (b) chemical weathering carbon sinks in carbonate rocks in each climatic zone. F-G, frigid grassland; F-D, frigid desert; FT-MCF, frigid temperate monsoon coniferous forest; SSTR-MRF, south subtropical monsoon rain forest; WTE-CG, warm temperate continental grassland; WTE-CD, warm temperate continental desert; WTE-MDBF, warm temperate monsoon deciduous broad-leaved forest; WTE-MFG, warm temperate monsoon forest and grassland; TK-RFMRF, tropical rain forest and monsoon rain forest; TE-G, temperate grassland; TE-D, temperate desert; TE-DBF, temperate deciduous broad-leaved forest; TE-FG, temperate forest and grassland; SF-G, sub-frigid grassland; MTE-CG, mid-temperate continental grassland; MTE-CDS, mid-temperate continental desert steppe; MTE-CD, mid-temperate monsoon coniferous and broad-leaved mixed forest; MSTR-MEBF, mid-subtropical monsoon evergreen broad-leaved forest; MSTR-MDEBF, north subtropical monsoon deciduous and evergreen broad-leaved forest.

zone, $23.17 t CO_2 km^{-2} yr^{-1}$ in the cool temperate zone, $7.22 t CO_2 km^{-2} yr^{-1}$ in the arid zone, and $6.64 t CO_2 km^{-2} yr^{-1}$ in the arid zone and the polar zone, which are lower than the global average of $29.08 t CO_2 km^{-2} yr^{-1}$ (Li C J et al., 2019). The main reason for this is that the chemical weathering process of carbonate rocks is closely related to the regional hydrothermal conditions. The high temperature and humidity conditions in the tropics promote the dissolution of carbonate rocks and accelerate the uptake of CO_2 . Moreover, the tropics are also the area where carbonate rocks are more concentrated, and it has been found that 13.1% of global carbonate rocks are distributed in the low-latitude tropics. In the low-latitude tropical areas in China, the distribution area of carbonate rocks accounts for 58.18% of the national carbonate rock distribution area, so its carbon sink flux is larger (Gaillardet et al., 2019). The high-latitude frigid and polar regions account for 36.8% of the global carbonate area, which is the main concentrated distribution area of carbonate rocks. In China, the frigid and subfrigid areas account for 18.52% of the national carbonate rock area. However, the low temperatures and relatively low precipitation in these areas greatly limit the CO_2 uptake during carbonate rock weathering (Rane, 2012; Xiong et al., 2022), ultimately leading to low carbon sink fluxes.

4.3 Comparison of results of different studies

The reliability of the calculation results was verified through comparison with the results of several related studies conducted at the regional and national scales. First, at the provincial scale, the CCSF for Guizhou Province was calculated to be $30.63 t CO_2 km^{-2} yr^{-1}$. The results of this study are similar to the results of other calculations using thermodynamic dissolution models, i.e., $30.3 t CO_2 km^{-2} yr^{-1}$ (Bai et al., 2023). Second, in this study, the CCSF for the southern karst area was calculated to be $33.14 t CO_2 km^{-2} yr^{-1}$, which is slightly lower than the results of other studies, i.e., $34.32 t CO_2 km^{-2} yr^{-1}$ (Zeng et al., 2016). This is mainly due to the fact that the chemical weathering of carbonate rocks is a fluctuating process, and there is some variability in the results of studies conducted on different time scales. In terms of both the totals and fluxes, the results of this study are generally consistent with or are within a reasonable range of the results of several studies conducted at the national scale (Table 3). In particular, our results are in general agreement with the CCSF calculated using the water chemical runoff method, the rock test piece method, and the thermodynamic dissolution model, demonstrating the reliability of our results. In addition, it should be noted that we only considered the distribution area of the carbonate rocks supported by

Table 3 Comparison of precision of research results

Research area	Methods	CCSF (t CO ₂ km ⁻² yr ⁻¹)	Area (10 ⁴ km ⁻²)	CCS (10 ⁴ t CO ₂ yr ⁻¹)	References
China	GEM-CO ₂ model	27.46	99.49	2732.00	Qiu et al. (2004)
China	Hydrochem-discharge (HD) method	19.14	344.00	6584.16	Liu and Zhao (2000)
China	Based on CRTT model	18.7	344.00	6432.80	Liu and Zhao (2000)
China	Maximal potential dissolution model	25.41	253.93	6452.36	Zeng and Liu (2022)
China	Maximal potential dissolution model	18.41	226.59	4171.52	Li H W et al. (2019)
China	Maximal potential dissolution model	22.76	155.06	3628.30	This study

basic data, which is about $252.98 \times 10^4 \text{ km}^{-2}$. In the karst area in Xizang autonomous region and the highland desert area in northwest China, the precipitation decreases significantly and the ET is strong, which lead to a decrease in soil moisture. This weakens the water quantity and dissolved CO₂ for the carbonate rock chemical weathering process. Under the conditions of the natural environment, it is difficult for weathering processes to occur, and therefore, these regions can hardly produce karst carbon sinks (Li H W et al., 2019). This is one of the reasons why the CCS calculated in this study is lower than the results of other studies.

In terms of the data selection and research methodology, first, the multi-year average ion concentration data of the major watersheds in China were obtained through a literature review. The problem of incomplete coverage of the ion concentration monitoring stations, which results in the data not reflecting the actual situation in China, was solved. Second, when using the model, we applied a mature and reliable thermodynamic dissolution model to evaluate the CCSF in China. The scientific validity of this model has been well verified (Hartmann et al., 2009; Zeng et al., 2016; Li et al., 2018, 2019; Börker et al., 2020; Zhang et al., 2021, 2022; Xiong et al., 2022), and it is one of the commonly used methods for assessing the CCSF.

In conclusion, this paper is reliable in terms of the use of data, the methodology, and the authenticity of the calculation results, and thus, it basically meets the accuracy requirements of similar studies.

4.4 Uncertainty and future outlook

Based on high-resolution spatial datasets, in this study, we determined the spatial pattern of the CCSF in China, and we systematically diagnosed and quantified the contributions of climate change, ecological restoration, and other factors to the CCSF. Although the data accuracy and methodological choices are similar to the results of previous studies, there are still some problems that need to be solved urgently. First, regarding the quantification of the CCSF, due to the difficulty of obtaining actual runoff depth for each pixel, the

difference between the MAP and ET was used to replace the actual runoff depth in the calculation process. Because the loss of precipitation due to industry and agriculture, evaporation, and infiltration was not considered, this may lead to a certain deviation of the regional CCSF from the actual value. Therefore, in the calculation process, we assigned a value of 0 to the negative values of the difference between the two, indicating that no karst inorganic carbon sink was generated. Second, in the selection of the influencing factors, the influences of macroscopic factors such as the MAP, MAT, ET, NDVI, and SM on the weathering process of carbonate rocks were focused on. Microscopic factors such as the organic matter content of the soil, exogenous acid, and exogenous water were not analyzed, which may affect the accuracy of the calculation results. In addition, the ecological restoration factors were mainly the NDVI and SM, which may reduce the precision of the evaluation of the contribution of each impact factor. Finally, in terms of the data accuracy selection, the accuracy of the main basic data we input is not yet high enough, which is the main source of uncertainty in the calculation results. In future research, we will comprehensively consider the influence mechanism of the chemical weathering rate of carbonate rocks, which will be combined with the optimized carbon sink measurement model in order to observe and predict the temporal evolution and the dynamic pattern of regional rock weathering carbon sinks and to simulate the contribution of the CCSF to achieving carbon neutrality under different scenarios. This will provide scientific data support for future research on carbon sources, sinks, and carbon neutrality.

5. Conclusions

In this study, we quantitatively determined the spatial pattern and influencing factors of the CCSF in China from 1991 to 2020 based on high-resolution hydrometeorological data, thermodynamic dissolution modeling, trend analysis, and partial derivatives. The main conclusions of this study are as follows.

(1) China's CCSF ($22.76 \text{ t CO}_2 \text{ km}^{-2} \text{ yr}^{-1}$) was higher than the global average ($15.77 \text{ t CO}_2 \text{ km}^{-2} \text{ yr}^{-1}$). With a carbonate rock area of $252.98 \times 10^4 \text{ km}^2$, it contributed 14.91% of the global CCS ($4772.67 \times 10^4 \text{ t CO}_2$).

(2) China's CCSF decreased gradually from southeast to northwest, with CCSF of 33.14, 12.93, and $7.27 \text{ t CO}_2 \text{ km}^{-2} \text{ yr}^{-1}$ in the southern karst, Qinghai-Tibetan karst, and northern karst regions, respectively.

(3) China's CCSF exhibited an overall increasing trend from 1991 to 2020, with a growth rate of $0.16 \text{ t CO}_2 \text{ km}^{-2} \text{ yr}^{-1}$.

(4) The MAP, MAT, ET, SM, and NDVI contributed 63.3%, 3.02%, 27.5%, 3.1%, and 3.05% to the CCSF, respectively.

The results of this study highlight that the CCSF is an indispensable component of the evaluation of the carbon neutral capacity of terrestrial ecosystems. Comprehensive quantification of the CCSF potentials and influencing factors in China and globally provides an important reference for solving the problem of the missing carbon sink and carbon imbalance in China and globally.

Acknowledgements This research work was supported by the National Natural Science Foundation (Grant Nos. U22A20619, 42077455 & 42367008), the Western Light Cross-team Program of Chinese Academy of Sciences (Grant No. xbzg-zdsys-202101), the Strategic Priority Research Program of the Chinese Academy of Sciences (Grant Nos. XDB40000000 & XDA23060100), the Guizhou Provincial Science and Technology Projects (Grant No. 2022-198), the High-level Innovative Talents in Guizhou Province (Grant Nos. GCC[2022]015-1 & 2016-5648), and the Guizhou Provincial Science and Technology Subsidies (Grant Nos. GZ2019SIG & GZ2020SIG).

Conflict of interest The authors declare that they have no conflict of interest.

References

- An Y L, Lü J M, Luo J, Wu Q X, Q L. 2018. Chemical weathering and CO_2 consumption of Chishuihe River Basin, Guizhou Province (in Chinese). *Adv Earth Sci*, 33: 179–188
- Anyamba A, Tucker C J. 2005. Analysis of Sahelian vegetation dynamics using NOAA-AVHRR NDVI data from 1981–2003. *J Arid Environ*, 63: 596–614
- Bai X Y, Zhang S R, Li C J, Xiong L, Song F J, Du C C, Li M H, Luo Q, Xue Y Y, Wang S J. 2023. A carbon-neutrality-capacity index for evaluating carbon sink contributions. *Environ Sci EcoTech*, 15: 100237
- Behzad H M, Arif M, Duan S, Kavousi A, Cao M, Liu J, Jiang Y. 2023. Seasonal variations in water uptake and transpiration for plants in a karst critical zone in China. *Sci Total Environ*, 860: 160424
- Börker J, Hartmann J, Amann T, Romero-Mujalli G, Moosdorf N, Jenkins C. 2020. Chemical weathering of loess and its contribution to global alkalinity fluxes to the coastal zone during the Last Glacial Maximum, Mid-Holocene, and Present. *Geochem Geophys Geosyst*, 21: e2020GC008922
- Cao J H, Jiang Z C, Yuan D X, Xia R Y, Zhang C. 2017. The progress in the study of the karst dynamic system and global changes in the past 30 years (in Chinese with English abstract). *Geol China*, 44: 874–900
- de Jong R, Schaepman M E, Furrer R, de Bruin S, Verburg P H. 2013. Spatial relationship between climatologies and changes in global vegetation activity. *Glob Change Biol*, 19: 1953–1964
- Drake T W, Tank S E, Zhulidov A V, Holmes R M, Gurtovaya T, Spencer R G M. 2018. Increasing alkalinity export from large Russian Arctic rivers. *Environ Sci Technol*, 52: 8302–8308
- Gaillardet J, Calmels D, Romero-Mujalli G, Zakharova E, Hartmann J. 2019. Global climate control on carbonate weathering intensity. *Chem Geol*, 527: 118762
- Gaillardet J, Dupré B, Louvat P, Allègre C J. 1999. Global silicate weathering and CO_2 consumption rates deduced from the chemistry of large rivers. *Chem Geol*, 159: 3–30
- Gao Y, Jia J J, Lu Y, Sun K, Wang J, Wang S Y. 2022. Carbon transportation, transformation, and sedimentation processes at the land-river-estuary continuum. *Fundamental Res*, 159: 3–30
- Ge W Y, Deng L Q, Wang F, Han J Q. 2021. Quantifying the contributions of human activities and climate change to vegetation net primary productivity dynamics in China from 2001 to 2016. *Sci Total Environ*, 773: 145648
- Gislason S R, Oelkers E H, Eiriksdottir E S, Kardjilov M I, Gisladdottir G, Sigfusson B, Snorrason A, Elefsen S O, Hardardottir J, Torssander P, Oskarsson N Ö. 2009. Direct evidence of the feedback between climate and weathering. *Earth Planet Sci Lett*, 277: 213–222
- Goldscheider N, Chen Z, Auler A S, Bakalowicz M, Broda S, Drew D, Hartmann J, Jiang G H, Moosdorf N, Stevanovic Z, Veni G. 2020. Global distribution of carbonate rocks and karst water resources. *Hydrogeol J*, 28: 1661–1677
- Gombert P. 2002. Role of karstic dissolution in global carbon cycle. *Glob Planet Change*, 33: 177–184
- Gong S H, Wang S J, Bai X Y, Luo G J, Wu L H, Chen F, Qian Q H, Xiao J Y, Zeng C. 2021. Response of the weathering carbon sink in terrestrial rocks to climate variables and ecological restoration in China. *Sci Total Environ*, 750: 141525
- Hartmann J, Jansen N, Dürr H H, Kempe S, Köhler P. 2009. Global CO_2 -consumption by chemical weathering: What is the contribution of highly active weathering regions? *Glob Planet Change*, 69: 185–194
- Jia J J, Gao Y, Sun K, Wang S Y, Wang J, Li Z X, Lu Y, Deng W Q, Ha X R. 2022. Drawdown zone can shift a floodplain-lake system from a steady carbon source to an unsteady carbon sink. *Agric For Meteorol*, 327: 109224
- Jiang Z C, Tan X Q, Cao J H, Jiang X Z, He S Y, Luo W Q. 2011. Calculation of atmospheric CO_2 sink formed in karst progresses of the karst divided regions in China (in Chinese). *Carsol Sin*, 30: 363–367
- Li C J, Bai X Y, Tan Q, Luo G J, Wu L H, Chen F, Xi H P, Luo X L, Ran C, Chen H, Zhang S R, Liu M, Gong S H, Xiong L, Song F J, Xiao B Q, Du C C. 2022. High-resolution mapping of the global silicate weathering carbon sink and its long-term changes. *Glob Change Biol*, 28: 4377–4394
- Li C J, Wang S J, Bai X Y, Tan Q, Li H W, Li Q, Deng Y H, Yang Y J, Tian S Q, Hu Z Y. 2019. Estimation of carbonate rocks weathering-related carbon sink in global major river basins (in Chinese). *Acta Geogr Sin*, 74: 1319–1332
- Li D T, Luo Y. 1983. Measurement of Carbonate Rocks Distribution Area in China (in Chinese). *Carsol Sin*, 2: 147
- Li H W, Wang S J, Bai X Y, Cao Y, Wu L H. 2019. Spatiotemporal evolution of carbon sequestration of limestone weathering in China. *Sci China Earth Sci*, 62: 974–991
- Li H W, Wang S J, Bai X Y, Luo W J, Tang H, Cao Y, Wu L H, Chen F, Li Q, Zeng C, Wang M M. 2018. Spatiotemporal distribution and national measurement of the global carbonate carbon sink. *Sci Total Environ*, 643: 157–170
- Li Q. 2020. Soil erosion process and its influence on organic carbon transport in China. Institute of Geochemistry, Chinese Academy of Sciences (in Chinese). The University of the Chinese Academy of Sciences
- Liu Z H, Dreybrodt W, Liu H. 2011. Atmospheric CO_2 sink: Silicate weathering or carbonate weathering? *Appl Geochem*, 26: S292–S294
- Liu Z H, Dreybrodt W, Wang H J. 2010. A new direction in effective

- accounting for the atmospheric CO₂ budget: Considering the combined action of carbonate dissolution, the global water cycle and photosynthetic uptake of DIC by aquatic organisms. *Earth-Sci Rev*, 99: 162–172
- Liu Z H, Macpherson G L, Groves C, Martin J B, Yuan D X, Zeng S B. 2018. Large and active CO₂ uptake by coupled carbonate weathering. *Earth-Sci Rev*, 182: 42–49
- Liu Z H, Zhao J. 2000. Contribution of carbonate rock weathering to the atmospheric CO₂ sink. *Environ Geol*, 39: 1053–1058
- Martin B, Kjeld R, Josep P, Feng T, Guy S, Aleixandre V, Ole M, Palmer J R B, Rasmus F. 2017. Human population growth offsets climate-driven increase in woody vegetation in sub-Saharan Africa. *Nat Ecol Evol*, 1: 0081
- Myneni R B, Keeling C D, Tucker C J, Asrar G, Nemani R R. 1997. Increased plant growth in the northern high latitudes from 1981 to 1991. *Nature*, 386: 698–702
- Peng S Z., Ding Y X., Liu W Z., Li Z. 2019. 1 km monthly temperature and precipitation dataset for China from 1901 to 2017. *Earth Syst Sci Data*, 11: 1931–1946
- Plummer L N, Busenberg E. 1982. The solubilities of calcite, aragonite and vaterite in CO₂-H₂O solutions between 0 and 90°C, and an evaluation of the aqueous model for the system CaCO₃-CO₂-H₂O. *Geochim Cosmochim Acta*, 46: 1011–1040
- Pu J B, Jiang Z C, Yuan D X, Zhang C. 2015. Some opinions on rock-weathering-related carbon sinks from the IPCC fifth assessment report (in Chinese). *Adv Earth Sci*, 30: 1081–1090
- Qiao Y, Jiang Y, Zhang C. 2021. Contribution of karst ecological restoration engineering to vegetation greening in southwest China during recent decade. *Ecol Indicators*, 121: 107081
- Qin C Q, Li S L, Yue F J, Ding H, Xu S, Liu C Q. 2021. Biogeochemical processes of dissolved carbon in the karst critical zone and its response to rainstorms (in Chinese). *Quat Sci*, 41: 1128–1139
- Qin X Q, Liu P Y, Huang Q B, Zhang L K. 2013. Estimation of Atmospheric/Soil CO₂ Consumption by Rock Weathering in the Pearl River Valley (in Chinese). *Acta Geosci Sin*, 34: 455–462
- Qiu D S, Zhuang D F, Hu Y F, Yao R. 2004. Estimation of Carbon Sink Capacity Caused by Rock Weathering in China. *Earth Science*, 29: 177–182, 190
- Rane L C. 2012. Carbon shifted but not sequestered. *Science*, 335: 655
- Raymond P A, Oh N H, Turner R E, Broussard W. 2008. Anthropogenically enhanced fluxes of water and carbon from the Mississippi River. *Nature*, 451: 449–452
- Sedano F, Lisboa S N, Duncanson L, Ribeiro N, Siteo A, Sahajpal R, Hurtt G, Tucker C J. 2020. Monitoring forest degradation from charcoal production with historical Landsat imagery. A case study in southern Mozambique. *Environ Res Lett*, 15: 015001
- Song X W, Gao Y, Wen X F, Guo D L, Yu G R, He N P, Zhang J Z. 2017. Carbon sequestration potential and its eco-service function in the karst area, China. *J Geogr Sci*, 27: 967–980
- Suchet P A, Probst J L, Ludwig W. 2003. Worldwide distribution of continental rock lithology: Implications for the atmospheric/soil CO₂ uptake by continental weathering and alkalinity river transport to the oceans. *Glob Biogeochem Cycle*, 17: 1038
- Sun H L, Liu Z H, Yang R, Chen B, Yang M X, Zeng Q G. 2017. Spatial and seasonal variations of hydrochemistry of the Peral River and implications for estimating the rock weathering-related carbon sink (in Chinese). *Earth Environ*, 45: 57–65
- White W B. 1984. Rate processes: Chemical kinetics and karst landform development. *Environ Sci Geol*, doi: 10.4324/9781003028833-10
- Xiao B Q, Bai X Y, Zhao C W, Tan Q, Li Y B, Luo G J, Wu L H, Chen F, Li C J, Ran C, Luo X L, Xi H P, Chen H, Zhang S R, Liu M, Gong S H, Xiong L, Song F J, Du C C. 2023. Responses of carbon and water use efficiencies to climate and land use changes in China's karst areas. *J Hydrol*, 617128968
- Xiao J Y, Xie B G, Zhou K C, Li J H, Xie J, Liang C. 2022. Contributions of climate change, vegetation growth, and elevated atmospheric CO₂ concentration to variation in water use efficiency in subtropical China. *Remote Sens*, 14: 4296
- Xie C J, Gao Q Z, Tao Z. 2012. Review and perspectives of the study on chemical weathering and hydrochemistry in river basin (in Chinese). *Trop Geogr*, 32: 331–337, 356
- Xiong L, Bai X Y, Zhao C W, Li Y B, Tan Q, Luo G J, Wu L H, Chen F, Li C J, Ran C, Xi H P, Luo X L, Chen H, Zhang S R, Liu M, Gong S H, Xiao B Q, Du C C, Song F J. 2022. High-resolution datasets for global carbonate and silicate rock weathering carbon sinks and their change trends. *Earths Future*, 10: e2022EF002746
- Ye T Z, Huang C K, Deng Z Q. 2017. Spatial database of 1:2500000 digital geologic map of People's Republic of China (in Chinese). *Geol China*, 44(S1): 19–24
- Yu Y, Bai J J, Wang J B, Wei H J. 2015. Analysis on spatio-temporal characteristics of ET based on MOD16 in Guanzhong Region (in Chinese). *Agric Res Arid Areas*, 33: 245–253
- Yuan D X. 2011. Review and prospect of geological processes and carbon cycle research. *Chin Sci Bull*, 56: 2157
- Zeng S B. 2017. Climate change characteristics of karst area in SW China and its impacts on karst-related carbon sink during recent 40 years (in Chinese). Dissertation for Master's Degree. Chongqing: Southwest University
- Zeng S B, Jiang Y J, Liu Z H. 2016. Assessment of climate impacts on the karst-related carbon sink in SW China using MPD and GIS. *Glob Planet Change*, 144: 171–181
- Zeng S B, Liu Z H. 2022. Karst-related carbon sink and the carbon neutral potential by carbonate liming in non-karst areas in China. *Chin Sci Bull*, 10: 5749
- Zeng S B, Liu Z H, Groves C. 2022. Large CO₂ removal by enhanced carbonate weathering from land-use changes. *Earth-science Reviews*, 225103915
- Zeng S B, Liu Z H, Kaufmann G. 2019. Sensitivity of the global carbonate weathering carbon-sink flux to climate and land-use changes. *Nat Commun*, 10: 5749
- Zhang S R, Bai X Y, Zhao C W, Tan Q, Luo G J, Wu L H, Xi H P, Li C J, Chen F, Ran C, Liu M, Gong S H, Song F J. 2022. China's carbon budget inventory from 1997 to 2017 and its challenges to achieving carbon neutral strategies. *J Clean Prod*, 347: 130966
- Zhang S R, Bai X Y, Zhao C W, Tan Q, Luo G J, Wang J F, Li Q, Wu L H, Chen F, Li C J, Deng Y H, Yang Y J, Xi H P. 2021. Global CO₂ consumption by silicate rock chemical weathering: Its past and future. *Earths Future*, 9: e2020EF001938

(Editorial handling: Jinzhi DING)